Research Article | Vol. 26, No. 6 | 19 Mar 2018 | OPTICS EXPRESS 7390
Optics EXPRESS

Sensor performance requirements for atmospheric correction of satellite ocean color remote sensing

MENGHUA WANG[1,*] AND HOWARD R. GORDON[2]

[1]NOAA National Environmental Satellite, Data, and Information Service, Center for Satellite Applications and Research, E/RA3, 5830 University Research Ct., College Park, Maryland 20740, USA
[2]Physics Department, University of Miami, Coral Gables, Florida, USA
[*]Menghua.Wang@noaa.gov

Abstract: We analyze the effects of the sensor signal-to-noise ratio (SNR) requirements for atmospheric correction of satellite ocean color remote sensing using the near-infrared (NIR) and shortwave infrared (SWIR) bands. Using the Gaussian noise model for the sensor noise distribution in the NIR and SWIR bands, some extensive simulations have been carried out to evaluate and assess the effects of sensor NIR and SWIR SNR values on the retrieved normalized water-leaving reflectance spectra $\rho_{wN}(\lambda)$, which are used to derive all ocean or inland water biological and biogeochemical property data. The standard atmospheric correction algorithm for global oceans and inland waters using the two NIR bands, i.e., Gordon and Wang (1994) [Appl. Opt. **33**, 443 (1994)], or two SWIR bands, i.e., Wang (2007) [Appl. Opt. **46**, 1535 (2007)], is assumed in the evaluation. Specifically, the minimum and goal SNR requirements for the NIR and SWIR bands for atmospheric correction are estimated. The minimum SNR values are those with which sufficiently accurate $\rho_{wN}(\lambda)$ can be derived, while the goal SNR requirements are those with which the atmospheric correction algorithms reach to their corresponding inherent limitations (or inherent errors), i.e., no gains can be achieved with further increase of SNR values in the NIR and SWIR bands. Evaluation results show that the minimum SNR requirement for the two NIR bands is ~200–300, while the minimum SNR requirement for the three SWIR bands is ~100. For the goal SNR requirements, the recommendations are SNR's of ~600 and ~200 for the two NIR bands and three SWIR bands, respectively.

OCIS codes: (010.0010) Atmospheric and oceanic optics; (010.1285) Atmospheric correction; (010.0280) Remote sensing and sensors; (010.4450) Oceanic optics.

References and links

1. H. R. Gordon, D. K. Clark, J. L. Mueller, and W. A. Hovis, "Phytoplankton Pigments from the Nimbus-7 Coastal Zone Color Scanner: Comparisons with Surface Measurements," Science **210**(4465), 63–66 (1980).
2. W. A. Hovis, D. K. Clark, F. Anderson, R. W. Austin, W. H. Wilson, E. T. Baker, D. Ball, H. R. Gordon, J. L. Mueller, S. Z. El-Sayed, B. Sturm, R. C. Wrigley, and C. S. Yentsch, "Nimbus-7 Coastal Zone Color Scanner: system description and initial imagery," Science **210**(4465), 60–63 (1980).
3. C. R. McClain, G. C. Feldman, and S. B. Hooker, "An overview of the SeaWiFS project and strategies for producing a climate research quality global ocean bio-optical time series," Deep Sea Res. Part II Top. Stud. Oceanogr. **51**(1-3), 5–42 (2004).
4. V. V. Salomonson, W. L. Barnes, P. W. Maymon, H. E. Montgomery, and H. Ostrow, "MODIS: advanced facility instrument for studies of the Earth as a system," IEEE Trans. Geosci. Remote Sens. **27**(2), 145–153 (1989).
5. W. E. Esaias, M. R. Abbott, I. Barton, O. B. Brown, J. W. Campbell, K. L. Carder, D. K. Clark, R. L. Evans, F. E. Hodge, H. R. Gordon, W. P. Balch, R. Letelier, and P. J. Minnet, "An overview of MODIS capabilities for ocean science observations," IEEE Trans. Geosci. Remote Sens. **36**(4), 1250–1265 (1998).
6. M. Rast, J. L. Bezy, and S. Bruzzi, "The ESA Medium Resolution Imaging Spectrometer MERIS a review of the instrument and its mission," Int. J. Remote Sens. **20**(9), 1681–1702 (1999).
7. M. D. Goldberg, H. Kilcoyne, H. Cikanek, and A. Mehta, "Joint Polar Satellite System: The United States next generation civilian polar-orbiting environmental satellite system," J. Geophys. Res. Atmos. **118**(24), 13463–13475 (2013).

#313464 https://doi.org/10.1364/OE.26.007390
Journal © 2018 Received 14 Nov 2017; revised 8 Feb 2018; accepted 8 Feb 2018; published 14 Mar 2018

Optics EXPRESS

8. M. Wang, X. Liu, L. Tan, L. Jiang, S. Son, W. Shi, K. Rausch, and K. Voss, "Impact of VIIRS SDR performance on ocean color products," J. Geophys. Res. Atmos. **118**(18), 10347–10360 (2013).
9. H. R. Gordon and M. Wang, "Retrieval of water-leaving radiance and aerosol optical thickness over the oceans with SeaWiFS: A preliminary algorithm," Appl. Opt. **33**(3), 443–452 (1994).
10. M. Wang, "Remote sensing of the ocean contributions from ultraviolet to near-infrared using the shortwave infrared bands: simulations," Appl. Opt. **46**(9), 1535–1547 (2007).
11. IOCCG, *Atmospheric Correction for Remotely-Sensed Ocean-Colour Products*, M. Wang, (Ed.), Reports of International Ocean-Color Coordinating Group, No. 10, IOCCG, Dartmouth, Canada (2010).
12. D. Antoine and A. Morel, "A multiple scattering algorithm for atmospheric correction of remotely sensed ocean colour (MERIS instrument): principle and implementation for atmospheres carrying various aerosols including absorbing ones," Int. J. Remote Sens. **20**(9), 1875–1916 (1999).
13. H. Fukushima, A. Higurashi, Y. Mitomi, T. Nakajima, T. Noguchi, T. Tanaka, and M. Toratani, "Correction of atmospheric effects on ADEOS/OCTS ocean color data: Algorithm description and evaluation of its performance," J. Oceanogr. **54**(5), 417–430 (1998).
14. H. R. Gordon, J. W. Brown, and R. H. Evans, "Exact Rayleigh scattering calculations for use with the Nimbus-7 Coastal Zone Color Scanner," Appl. Opt. **27**(5), 862–871 (1988).
15. M. Wang, "A refinement for the Rayleigh radiance computation with variation of the atmospheric pressure," Int. J. Remote Sens. **26**(24), 5651–5663 (2005).
16. M. Wang, "Rayleigh radiance computations for satellite remote sensing: Accounting for the effect of sensor spectral response function," Opt. Express **24**(11), 12414–12429 (2016).
17. H. R. Gordon and M. Wang, "Influence of oceanic whitecaps on atmospheric correction of ocean-color sensors," Appl. Opt. **33**(33), 7754–7763 (1994).
18. R. Frouin, M. Schwindling, and P. Y. Deschamps, "Spectral reflectance of sea foam in the visible and near infrared: In situ measurements and remote sensing implications," J. Geophys. Res. **101**(C6), 14361–14371 (1996).
19. K. D. Moore, K. J. Voss, and H. R. Gordon, "Spectral reflectance of whitecaps: Their contribution to water-leaving radiance," J. Geophys. Res. **105**(C3), 6493–6499 (2000).
20. M. Wang and S. W. Bailey, "Correction of the sun glint contamination on the SeaWiFS ocean and atmosphere products," Appl. Opt. **40**(27), 4790–4798 (2001).
21. H. R. Gordon, T. Du, and T. Zhang, "Remote sensing of ocean color and aerosol properties: resolving the issue of aerosol absorption," Appl. Opt. **36**(33), 8670–8684 (1997).
22. F. Steinmetz, P. Y. Deschamps, and D. Ramon, "Atmospheric correction in presence of sun glint: application to MERIS," Opt. Express **19**(10), 9783–9800 (2011).
23. T. Shroeder, I. Behnert, M. Schaale, J. Fischer, and R. Doerffer, "Atmospheric correction algorithm for MERIS above case-2 waters," Int. J. Remote Sens. **28**(7), 1469–1486 (2007).
24. M. Wang and W. Shi, "Estimation of ocean contribution at the MODIS near-infrared wavelengths along the east coast of the U.S.: Two case studies," Geophys. Res. Lett. **32**(13), L13606 (2005).
25. M. Wang and W. Shi, "The NIR-SWIR combined atmospheric correction approach for MODIS ocean color data processing," Opt. Express **15**(24), 15722–15733 (2007).
26. M. Wang, S. Son, and W. Shi, "Evaluation of MODIS SWIR and NIR-SWIR atmospheric correction algorithm using SeaBASS data," Remote Sens. Environ. **113**(3), 635–644 (2009).
27. D. A. Siegel, M. Wang, S. Maritorena, and W. Robinson, "Atmospheric correction of satellite ocean color imagery: the black pixel assumption," Appl. Opt. **39**(21), 3582–3591 (2000).
28. K. G. Ruddick, F. Ovidio, and M. Rijkeboer, "Atmospheric correction of SeaWiFS imagery for turbid coastal and inland waters," Appl. Opt. **39**(6), 897–912 (2000).
29. S. J. Lavender, M. H. Pinkerton, G. F. Moore, J. Aiken, and D. Blondeau-Patissier, "Modification to the atmospheric correction of SeaWiFS ocean color images over turbid waters," Cont. Shelf Res. **25**(4), 539–555 (2005).
30. W. Shi and M. Wang, "Ocean reflectance spectra at the red, near-infrared, and shortwave infrared from highly turbid waters: A study in the Bohai Sea, Yellow Sea, and East China Sea," Limnol. Oceanogr. **59**(2), 427–444 (2014).
31. W. Shi and M. Wang, "An assessment of the black ocean pixel assumption for MODIS SWIR bands," Remote Sens. Environ. **113**(8), 1587–1597 (2009).
32. J. Sun and M. Wang, "Radiometric calibration of the VIIRS reflective solar bands with robust characterizations and hybrid calibration coefficients," Appl. Opt. **54**, 9331–9342 (2015).
33. H. R. Gordon, "In-orbit calibration strategy for ocean color sensors," Remote Sens. Environ. **63**(3), 265–278 (1998).
34. B. A. Franz, S. W. Bailey, P. J. Werdell, and C. R. McClain, "Sensor-independent approach to the vicarious calibration of satellite ocean color radiometry," Appl. Opt. **46**(22), 5068–5082 (2007).
35. M. Wang, W. Shi, L. Jiang, and K. Voss, "NIR- and SWIR-based on-orbit vicarious calibrations for satellite ocean color sensors," Opt. Express **24**(18), 20437–20453 (2016).
36. G. Zibordi, F. Melin, K. Voss, B. C. Johnson, B. A. Franz, E. Kwiatkowska, J. P. Huot, M. Wang, and D. Antoine, "System vicarious calibration for ocean color climate change applications: Requirements for in situ data," Remote Sens. Environ. **159**, 361–369 (2015).

Optics EXPRESS

37. G. Thuillier, M. Herse, D. Labs, T. Foujols, W. Peetermans, D. Gillotay, P. C. Simon, and H. Mandel, "The solar spectral irradiance from 200 to 2400 nm as measured by the SOLSPEC spectrometer from the ATLAS and EURECA missions," Sol. Phys. **214**(1), 1–22 (2003).
38. E. P. Shettle and R. W. Fenn, "Models for the Aerosols of the Lower Atmosphere and the Effects of Humidity Variations on Their Optical Properties," (U.S. Air Force Geophysics Laboratory, Hanscom Air Force Base, Mass., 1979), pp. 1–94.
39. M. Wang, "Aerosol polarization effects on atmospheric correction and aerosol retrievals in ocean color remote sensing," Appl. Opt. **45**(35), 8951–8963 (2006).
40. M. Wang, K. D. Knobelspiesse, and C. R. McClain, "Study of the Sea-Viewing Wide Field-of-View Sensor (SeaWiFS) aerosol optical property data over ocean in combination with the ocean color products," J. Geophys. Res. **110**, D10S06 (2005).
41. A. A. Gitelson, J. F. Schalles, and C. M. Hladik, "Remote chlorophyll-a retrieval in turbid, productive estuaries: Chesapeake Bay case study," Remote Sens. Environ. **109**(4), 464–472 (2007).
42. M. Wang, S. Son, and J. L. W. Harding, Jr., "Retrieval of diffuse attenuation coefficient in the Chesapeake Bay and turbid ocean regions for satellite ocean color applications," J. Geophys. Res. **114**(C10), C10011 (2009).
43. C. Hu, L. Feng, Z. Lee, C. O. Davis, A. Mannino, C. R. McClain, and B. A. Franz, "Dynamic range and sensitivity requirements of satellite ocean color sensors: learning from the past," Appl. Opt. **51**(25), 6045–6062 (2012).
44. C. R. McClain, "A decade of satellite ocean color observations," Annu. Rev. Mar. Sci. **1**(1), 19–42 (2009).
45. L. Qi, Z. Lee, C. Hu, and M. Wang, "Requirement of minimal signal-to-noise ratios of ocean color sensors and uncertainties of ocean color products," J. Geophys. Res. Oceans **122**(3), 2595–2611 (2017).
46. C. Cao, X. Xiong, S. Blonski, Q. Liu, S. Uprety, X. Shao, Y. Bai, and F. Weng, "Suomi NPP VIIRS sensor data record verification, validation, and long-term performance monitoring," J. Geophys. Res. Atmos. **118**(20), 11664–11678 (2013).
47. M. Wang and W. Shi, "Sensor noise effects of the SWIR bands on MODIS-derived ocean color products," IEEE Trans. Geosci. Remote Sens. **50**(9), 3280–3292 (2012).
48. S. Son and M. Wang, "Water properties in Chesapeake Bay from MODIS-Aqua measurements," Remote Sens. Environ. **123**, 163–174 (2012).
49. M. Wang, W. Shi, and J. Tang, "Water property monitoring and assessment for China's inland Lake Taihu from MODIS-Aqua measurements," Remote Sens. Environ. **115**(3), 841–854 (2011).
50. W. Shi and M. Wang, "Satellite observations of flood-driven Mississippi River plume in the spring of 2008," Geophys. Res. Lett. **36**(7), L07607 (2009).
51. W. Shi and M. Wang, "Satellite views of the Bohai Sea, Yellow Sea, and East China Sea," Prog. Oceanogr. **104**, 35–45 (2012).

1. Introduction

Ocean color satellite remote sensing was started with the NASA Coastal Zone Color Scanner (CZCS) [1, 2] as a proof-of-concept mission which demonstrated the feasibility of *quantitative* retrieval of ocean near-surface optical and biological property data. Since the success of the CZCS mission, several ocean color satellite sensors capable of routine global ocean color coverage have been launched, e.g., the Sea-viewing Wild Field-of-view Sensor (SeaWiFS) (1997–2010) [3], the Moderate Resolution Imaging Spectroradiometer (MODIS) [4, 5] on the Terra (1999–present) and Aqua (2002–present) satellites, the Medium-Resolution Imaging Spectrometer (MERIS) [6] on the Envisat (2002–2012), the Visible Infrared Imaging Radiometer Suite (VIIRS) [7, 8] on the Suomi National Polar-orbiting Partnership (SNPP) (2011–present) and NOAA-20 (2017–present), the Ocean and Land Color Instrument (OLCI) on the Sentinel-3 (2016–present), and the Second-Generation Global Imager (SGLI) on the Global Change Observation Mission-Climate (GCOM-C) (2017–present). Indeed, we now have unprecedented routine view of ocean optical, biological, and biogeochemical properties on global scales by using the state-of-the-art algorithms to process satellite data, providing useful satellite ocean color observations for research and various applications.

In satellite ocean color remote sensing, atmospheric correction is the key data processing procedure that removes radiance contributions from the atmosphere and ocean surface [9–13]. Briefly, the standard atmospheric correction algorithm, which has been used for over twenty years of successful satellite global ocean color data processing (SeaWiFS, MODIS, and VIIRS) uses two near-infrared (NIR) bands to estimate radiance contributions from aerosols and Rayleigh-aerosol interactions and then extrapolates the effects to the visible bands [9–11]. This is after corrections of radiance contributions from molecules (Rayleigh scattering)

Optics EXPRESS

[14–16], ocean whitecaps [17–19], and sun glint [20]. There are also other atmospheric correction approaches implemented in the routine satellite ocean color data processing, e.g., the spectral matching algorithm [21, 22], and the neural network approach for coastal regions [23]. For open oceans, the water-leaving radiance contributions at the NIR bands are negligible (i.e., the black ocean assumption) [9]. The aerosol contribution effects are assessed in the NIR and then removed from the visible bands. It should be noted that the extrapolation of the aerosol effects from the NIR to visible uses the realistic aerosol models and radiances computed from radiative transfer model simulations for the ocean-atmosphere system. Over turbid coastal and inland waters, however, it has been shown that the shortwave infrared (SWIR) bands should be used for atmospheric correction in processing satellite ocean color data [10, 24–26], because over turbid waters the water-leaving radiances at the NIR bands are no longer negligible [27–29], and even significant for highly turbid waters [30]. Thus, for highly turbid waters SWIR bands can be used for atmospheric correction with the assumption of the black ocean at the SWIR bands [31].

It is obvious that for the standard atmospheric correction satellite ocean color results depend on the accuracy of the sensor-measured top-of-atmosphere (TOA) radiance at the NIR (or SWIR) bands, i.e., sensor on-orbit radiometer calibration [32] and system vicarious calibrations [33–36] as well as sensor noise error in the NIR (or SWIR) bands. All errors in the NIR (or SWIR) bands will pass through atmospheric correction into the visible bands, showing up as errors in the satellite-derived normalized water-leaving reflectance spectra $\rho_{wN}(\lambda)$. In turn, satellite-derived biological and biogeochemical products that are derived from $\rho_{wN}(\lambda)$ spectra will also have errors that are inherent to the atmospheric correction algorithm itself. It is noted that the relationship between the reflectance and the radiance is as follows: for any radiance L in the atmosphere-ocean system the associated reflectance ρ is related to L by $\rho = \pi L/(F_0 \cos\theta_0)$, where F_0 is the extraterrestrial solar irradiance [37], in the same spectral band as L, and θ_0 is the solar-zenith angle. Post-launch sensor calibrations (i.e., on-orbit radiometric and vicarious calibrations) can be improved during the post-launch period, while the sensor signal-to-noise ratio (SNR) performance is completely determined in the pre-launch sensor design stage. The sensor SNR characteristics cannot be improved after the sensor is in-orbit (and usually will be getting worse, i.e., degrading with time). Therefore, it is important to have appropriate sensor SNR values for the NIR and SWIR bands in order to have accurate satellite ocean color products.

There are two SNR requirements discussed in this study. First, the required NIR and SWIR SNR values for atmospheric correction to derive sufficiently accurate $\rho_{wN}(\lambda)$ spectra for general global ocean color applications. Specifically, we use the 5% uncertainty in $\rho_{wN}(\lambda)$ at the blue 443 nm band for clear open ocean waters, which can be used to derive the chlorophyll-a concentration within ~35% [9]. For this case, the required reflectance uncertainty $\Delta\rho_{wN}(\lambda)$ at the blue is ~1–2 × 10^{-3} [9–11]. This provides the minimum SNR requirements for the NIR and SWIR bands for global ocean color remote sensing. However, in the case of the SWIR bands, the open ocean criterion may have limited applicability for turbid coastal and inland waters. We will discuss this in more detail in Section 3.2.

The second criteria used in this study is for fully utilizing the state-of-the-art atmospheric correction performance accuracy for deriving $\rho_{wN}(\lambda)$ spectra, and the sensor NIR and SWIR required SNR values are those that, with such SNR values, the uncertainty $\Delta\rho_{wN}(\lambda)$ reaches the algorithm inherent errors, i.e., with further increase of sensor NIR or SWIR SNR values there are no gains to be achieved for improving satellite-derived $\rho_{wN}(\lambda)$ spectra. We use the goal SNR requirement for the second one. Obviously, the first SNR requirements (minimum) for the NIR and SWIR bands are usually less than the second ones (goal requirements).

In this paper, we analyze the sensor SNR effect in the NIR and SWIR bands on the accuracy of the derived normalized water-leaving reflectance spectra $\rho_{wN}(\lambda)$. Assuming that the sensor noise follows a Gaussian distribution, uncertainty of the satellite-derived $\rho_{wN}(\lambda)$ spectra can be simulated with various levels of sensor SNR values at the NIR and SWIR

Optics EXPRESS

bands that are used for atmospheric correction. Therefore, the required sensor SNR values for the NIR and SWIR bands for satellite ocean color remote sensing can be estimated.

2. Methodology

In this section, we describe our approach to evaluate effects of the sensor SNR values at the NIR and SWIR bands, which are used for atmospheric correction, on the satellite-derived $\rho_{wN}(\lambda)$ spectra. A Gaussian noise model and some detailed results from the NIR atmospheric correction [9] using 765 and 865 nm and the SWIR atmospheric correction [10] using the SWIR band sets of 1240 & 1640 nm, 1240 & 2130 nm, and 1640 & 2130 nm are described and discussed.

2.1. Noise model for the sensor SNR values

Let the measured TOA reflectance be denoted by $\rho_t^{(M)}(\lambda)$ and the true (noise free) reflectance by $\rho_t(\lambda)$. Then

$$\rho_t^{(M)}(\lambda) = \rho_t(\lambda) + \Delta\rho_t(\lambda) \tag{1}$$

where $\Delta\rho_t(\lambda)$ is the noise-induced error in the measured $\rho_t^{(M)}(\lambda)$. The noise error $\Delta\rho_t(\lambda)$ is a random variable, which we assume has a Gaussian distribution with mean zero and variance $(NE\Delta\rho_t(\lambda))^2$, where $NE\Delta\rho_t(\lambda)$ is called the "noise-equivalent reflectance." The SNR is then defined to be

$$SNR \equiv \frac{\rho_t(\lambda)}{NE\Delta\rho_t(\lambda)}, \tag{2}$$

i.e., the true signal ($\rho_t(\lambda)$) divided by the standard deviation (STD) of the noise-associated fluctuations. Note that the $NE\Delta\rho_t(\lambda)$ is usually some function of $\rho_t(\lambda)$ itself, e.g., for shot noise or photon noise, $NE\Delta\rho_t(\lambda) \propto \sqrt{\rho_t(\lambda)}$, so it is important to know at what value of $\rho_t(\lambda)$ the SNR is specified. The values of $\rho_t(\lambda)$ used in this study are provided in Section 2.3. Thus, to simulate the noise in a given spectral band, we repeatedly sample $\Delta\rho_t(\lambda)$ from the probability density

$$p\left(\Delta\rho_t(\lambda)\right) = \frac{1}{\sqrt{2\pi\sigma^2}} exp\left[-\frac{1}{2}\left(\frac{\Delta\rho_t(\lambda)}{\sigma}\right)^2\right], \tag{3}$$

where $\sigma = NE\Delta\rho_t(\lambda)$. Each sample is then added to $\rho_t(\lambda)$ to form $\rho_t^{(M)}(\lambda)$—an individual sample of the measured reflectance. Here, we choose a value for the SNR and from Eq. (2) compute the required $NE\Delta\rho_t(\lambda)$. In this study, the SNR's of the two bands used in the atmospheric correction algorithm are taken to be the same, e.g., the SNR's at the two NIR bands (765 and 865 nm in SeaWiFS) or two SWIR bands (1240 and 2130 nm in MODIS) are identical. Note that this means that the $NE\Delta\rho_t(\lambda)$'s are *not* the same because their $\rho_t(\lambda)$'s will be different. In addition, the $\Delta\rho_t(\lambda)$'s of the two correction bands are uncorrelated, i.e., they are chosen *separately* from their respective probability densities. Eight noise levels are generated, corresponding to SNR's of 25, 50, 100, 200, 400, 600, 800, and 1000. It is noted that the reflectance noise is *only* added into the bands that are used for atmospheric correction (e.g., two NIR bands or the SWIR bands), and UV (340 nm) and visible bands are noise free in all simulations discussed in this section. In other words, the study is to understand the impact of SNR values (or noise errors) of the NIR or SWIR bands, which are used for atmospheric correction, on the satellite-derived $\rho_{wN}(\lambda)$ spectra at the UV and visible bands.

Optics EXPRESS

2.2. Atmospheric correction

Atmospheric correction simulations using two NIR bands with the *Gordon and Wang* (1994) algorithm [9] and various options with the SWIR bands as outlined by *Wang* (2007) [10] have been carried out including reflectance noise levels for the corresponding NIR and SWIR bands. In atmospheric correction simulations, the aerosol lookup tables (LUTs) were generated using the 12 aerosol models derived from the work of *Shettle and Fenn* (1979) [38]. Specifically, they are the Oceanic model with relative humidity (RH) of 99% (O99), the Maritime models with RH of 50%, 70%, 90%, and 99% (M50, M70, M90, M99), the Coastal models with RH of 50%, 70%, 90%, and 99% (C50, C70, C90, C99), and the Tropospheric models with RH of 50%, 90%, and 99% (T50, T90, T99) [9, 10, 38]. The aerosol LUTs (12 aerosol models) contain the fitting coefficients for a large number of solar-sensor geometries (including all possible solar-sensor geometries in satellite remote sensing) and for values of the aerosol optical thicknesses (AOTs) from 0.02 to 0.8 [10]. In addition, the aerosol LUTs were generated including the polarization effects [39]. In fact, similar aerosol LUTs have been used in the Multi-Sensor Level-1 to Level-2 (MSL12) ocean color data processing system for routine production of VIIRS global ocean color products [8]. MSL12 is an official NOAA VIIRS ocean color data processing system. VIIRS-SNPP mission-long global ocean color product images using the NIR-, SWIR-, and NIR-SWIR-based atmospheric corrections and some extensive calibration and validation results can be found at (https://www.star.nesdis.noaa.gov/sod/mecb/color/).

For atmospheric correction simulations, the pseudo TOA reflectance data were generated using the two aerosol models that are different (although similar) from the aerosol LUTs that are used for atmospheric correction. Specifically, simulations were carried out for a typical Maritime aerosol model with a RH of 80% (M80) and a Tropospheric aerosol model with a RH of 80% (T80), where the T80 model is actually the M80 model without the large particle size fraction [38], for AOTs at 865 nm of 0.05, 0.1, 0.2, and 0.3. It should be particularly noted again that the M80 and T80 aerosol models were not used in the aerosol LUTs for atmospheric correction [9, 10]. Simulations were performed for a case with solar-zenith angle of 60°, sensor-zenith angle of 45°, and relative-azimuth angle of 90°. This solar-sensor geometry represents a typical case for atmospheric correction simulation results [9, 10].

2.3. The TOA reflectance

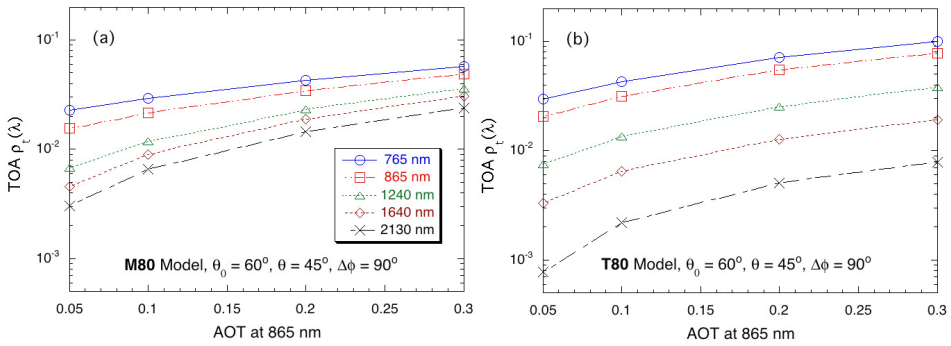

Fig. 1. TOA $\rho_t(\lambda)$ as a function of AOT at 865 nm for the NIR and SWIR bands that are used in atmospheric corrections for the SNR evaluation in the all cases in this study for the aerosol model of (a) M80 and (b) T80.

As the noise equivalent reflectance for many noise sources is a function of the reflectance itself, it is important to know the actual value of the reflectance at which the SNR is

Optics EXPRESS

evaluated. To effect this, in Fig. 1, we provide the true reflectance in the NIR and SWIR bands as a function of AOT at 865 nm, $\tau_a(865)$, for the all cases examined in this study.

2.4. Simulations

For each case, atmospheric correction for 5000 noise realizations with a given SNR value was carried out. For example, for a case with AOT at 865 nm, $\tau_a(865)$, of 0.1, 5000 reflectance noise samples (with a given SNR value) were generated and added into the TOA NIR (765 and 865 nm) reflectance values as shown in Fig. 1. The *Gordon and Wang* (1994) [9] NIR atmospheric correction algorithm was then performed 5000 times to generate the corresponding $\rho_{wN}(\lambda)$ spectra error $\Delta\rho_{wN}(\lambda)$. The same procedure was carried out for all four AOTs and also for the SWIR atmospheric correction algorithm using various SWIR band sets [10]. In the SWIR atmospheric correction, however, the Gaussian noise was of course added into the specific two SWIR bands (error free for UV to NIR bands), which are used for the SWIR atmospheric correction [10]. This produces the uncertainty in the derived $\rho_{wN}(\lambda)$ spectra from the UV (340 nm) to the red (or NIR in the case of the SWIR atmospheric correction). In effect, the simulated uncertainty $\Delta\rho_{wN}(\lambda)$ spectra include errors inherent to the atmospheric correction algorithm (i.e., errors discussed in *Gordon and Wang* (1994) [9] for the NIR-based algorithm and *Wang* (2007) [10] for the SWIR-based algorithm) and errors resulted from the added Gaussian noise in the NIR or SWIR bands used for atmospheric correction.

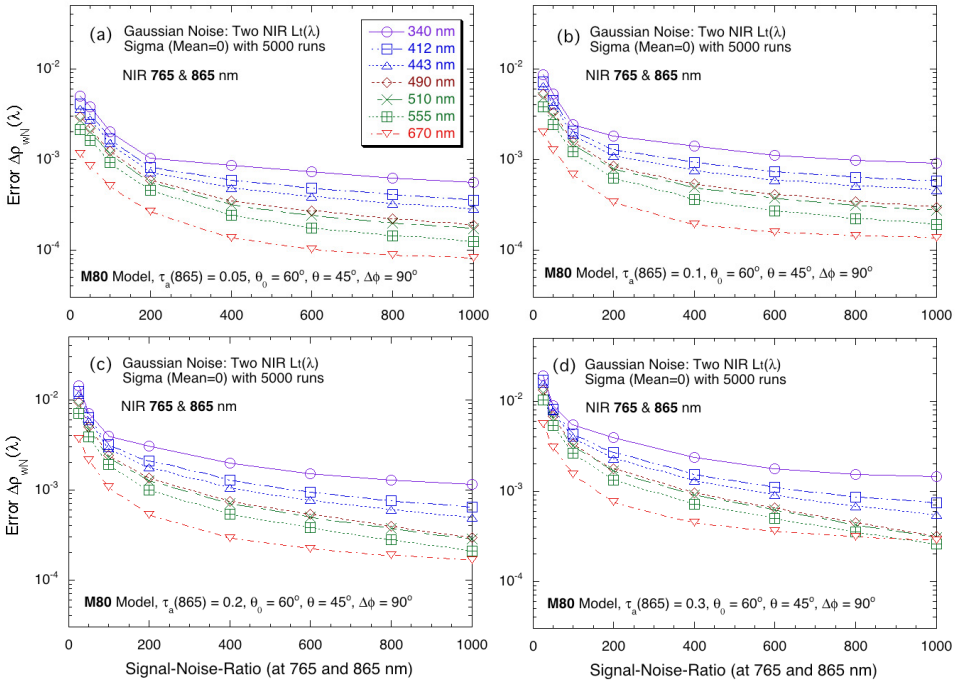

Fig. 2. Error $\Delta\rho_{wN}(\lambda)$ for wavelengths of the UV (340 nm) to red (670 nm) as a function of the SNR value using the NIR atmospheric correction for the M80 aerosol model with AOT at 865 nm of (a) 0.05, (b) 0.1, (c) 0.2, and (d) 0.3.

Optics EXPRESS

3. Results

3.1. Simulation results from the NIR atmospheric correction

Figures 2 and 3 provide sample results in the normalized water-leaving reflectance uncertainty spectra $\Delta\rho_{wN}(\lambda)$ (UV to red) as a function of the SNR value with simulations from the NIR atmospheric correction for aerosols modeled as M80 and T80, respectively. Two NIR bands at 765 and 865 nm are used for atmospheric correction [9]. The error in the normalized water-leaving reflectance, $\Delta\rho_{wN}(\lambda)$, is actually the STD value of the derived uncertainty in $\rho_{wN}(\lambda)$ over the 5000 Gaussian noise realizations, i.e., each point in the plot in Figs. 2 and 3 was derived from 5000 simulations ($\rho_{wN}(\lambda)$). The STD error was computed assuming that the mean value = 0 (i.e., error free). In this manner, when the NIR bands are noise free, $\Delta\rho_{wN}(\lambda)$ will reduce to the inherent error in the atmospheric correction algorithm. Figures 2(a)–2(d) are results for the NIR atmospheric correction with the M80 aerosol model for AOT values at the wavelength of 865 nm $\tau_a(865)$ of 0.05, 0.1, 0.2, and 0.3, respectively, while Figs. 3(a)–3(d) are similar results for the T80 aerosol model.

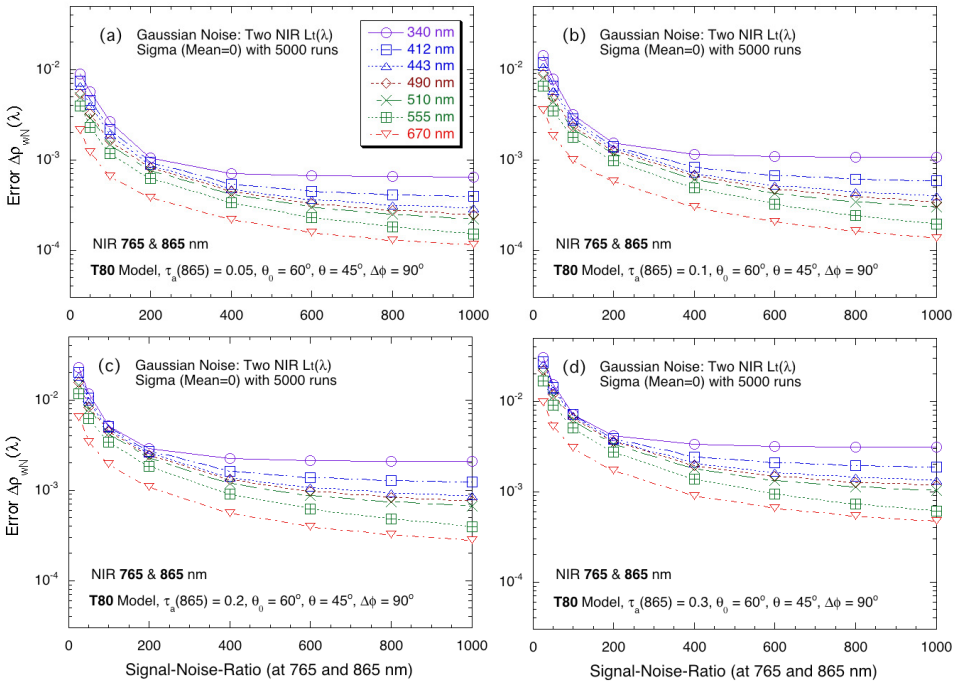

Fig. 3. Error $\Delta\rho_{wN}(\lambda)$ for wavelengths of the UV (340 nm) to red (670 nm) as a function of the SNR value using the NIR atmospheric correction for the T80 aerosol model with AOT at 865 nm of (a) 0.05, (b) 0.1, (c) 0.2, and (d) 0.3.

Results in Figs. 2 and 3 show that, as expected, error $\Delta\rho_{wN}(\lambda)$ decreases with increase of the SNR value in the two NIR bands (or decrease of the sensor noise error), and they reach to the inherent NIR atmospheric correction errors (i.e., algorithm errors) [9] with large enough SNR values. The NIR atmospheric correction algorithm generally performed slightly better for lower AOT values for both M80 and T80 models (as expected) [9]. For the M80 aerosol model (Fig. 2), the error $\Delta\rho_{wN}(\lambda)$ is actually flatted out (constant) at about SNR value of 600, in particular, $\Delta\rho_{wN}(\lambda)$ for all spectral bands is less than 10^{-3}, i.e., ~10^{-3} for the UV 340 nm band and ~10^{-4} for the red 670 nm band. For the T80 aerosol model (Fig. 3), the reflectance error $\Delta\rho_{wN}(\lambda)$ is flatted out at a slightly lower SNR value, in particular, for the UV 340 nm

Optics EXPRESS

band (at SNR of ~400–500). However, at an SNR of 600, the performance of the NIR atmospheric correction is improved for the longer spectral bands, e.g., for the green and red bands (Fig. 3). Thus, if the NIR SNR value is > ~600, there are no gains to be achieved with further increase of the SNR at the two NIR bands. This is the "goal" SNR.

For the minimum NIR SNR requirement, we can use the $\Delta\rho_{wN}(\lambda)$ at 443 nm, $\Delta\rho_{wN}(443)$, from results in Figs. 2 and 3. Specifically, Figs. 2(b) and 3(b) show that, for $\tau_a(865)$ of 0.1, $\Delta\rho_{wN}(443)$ reaches ~1–2 × 10^{-3} with an SNR value of ~200 for both the M80 and T80 models. For larger $\tau_a(865)$ values (e.g., 0.2 and 0.3), larger SNR values for the NIR bands are required, particularly for the T80 aerosols [Figs. 3(c) and 3(d)]. Results show that, with the NIR SNR values of ~200–300, $\Delta\rho_{wN}(443)$ can get to ~1–2 × 10^{-3}. This is the "minimum" SNR requirement for the sensor NIR bands for the NIR atmospheric correction. For lower SNR values, $\Delta\rho_{wN}(443)$ becomes a strong function of its actual value.

In summary, results in Figs. 2 and 3 show that, for the NIR atmospheric correction [9], the minimum sensor NIR SNR requirement is > ~200–300 and the goal SNR requirement is > ~600.

3.2. Simulation results from the SWIR atmospheric correction

The SWIR bands are used for atmospheric corrections in coastal areas where $\rho_{wN}(\lambda)$ cannot be taken to be zero in the NIR. These waters range from (1) having bio-optical properties similar to those in the open ocean but with a higher concentration of constituents, yielding reflectance spectra depressed in the blue and enhanced in the red, to (2) waters with high concentrations of mineral particles (resuspended from the bottom or introduced by runoff from land via rivers), which may have enhanced reflectance throughout the visible spectrum. The $\rho_{wN}(\lambda)$ spectrum in coastal waters is therefore either specific to the site or to the process under study. Thus, the criteria we used to assess the *minimum* SNR for the SWIR bands (i.e., $\Delta\rho_{wN}(\lambda)$ less than ~1–2 × 10^{-3} at 443 nm [9–11]) will be inadequate for all coastal waters; however, our simulation results are presented in such a manner that given the $\rho_{wN}(\lambda)$ accuracy requirement for any spectral band, the minimum SNR needed to achieve that accuracy can be determined immediately. Of course, the *goal* SNR, which depends only on the inherent error in the atmospheric correction algorithm, is independent of the properties of the water and is the same for open ocean and turbid coastal waters.

Similar to the simulations for the NIR atmospheric correction [9], the SNR effects on the SWIR atmospheric correction [10] for satellite-derived $\rho_{wN}(\lambda)$ spectra have also been carried out. Again, for each case, the SWIR atmospheric correction for 5000 noise realizations with a given SNR value to the corresponding two SWIR bands was carried out. For each case, 5000 reflectance noise samples (with a given SNR value) were generated and added into the corresponding two TOA SWIR reflectance values shown in Fig. 1. The SWIR atmospheric correction [10] was then performed 5000 times to generate the corresponding normalized water-leaving reflectance spectra error $\Delta\rho_{wN}(\lambda)$. Figure 4 shows results of the spectral reflectance error $\Delta\rho_{wN}(\lambda)$ from the UV (340 nm) to the NIR (865 nm) as a function of the SNR value for the three combinations of the SWIR band sets for the SWIR atmospheric correction [10]. Results in Fig. 4 are for both the M80 [Figs. 4(a), 4(c), and 4(e)] and T80 [Figs. 4(b), 4(d), and 4(f)] models, and for an AOT of 0.1 at 865 nm, which is near the average value over the global ocean [40]. The three combinations of the SWIR band sets for atmospheric correction are the SWIR bands 1240 and 1640 nm [Figs. 4(a) and 4(b)], 1240 and 2130 nm [Figs. 4(c) and 4(d)], and 1640 and 2130 nm [Figs. 4(e) and 4(f)]. Detailed analyses for the SWIR-based atmospheric correction performance (i.e., algorithm inherent errors) for the three SWIR approaches (i.e., using the SWIR bands 1240 & 1640 nm, 1240 & 2130 nm, and 1640 & 2130 nm) are provided in *Wang* (2007) [10]. It shows that atmospheric correction using the SWIR band sets of 1240 & 1640 nm and 1240 & 2130 nm can generally produce results comparable to those using the NIR bands (765 & 865 nm) [10]. The $\rho_{wN}(\lambda)$

Optics EXPRESS

spectra derived from the SWIR band set of 1640 & 2130 nm are slightly poorer [10]. Indeed, results from Fig. 4 are consistent with those of *Wang* (2007) [10].

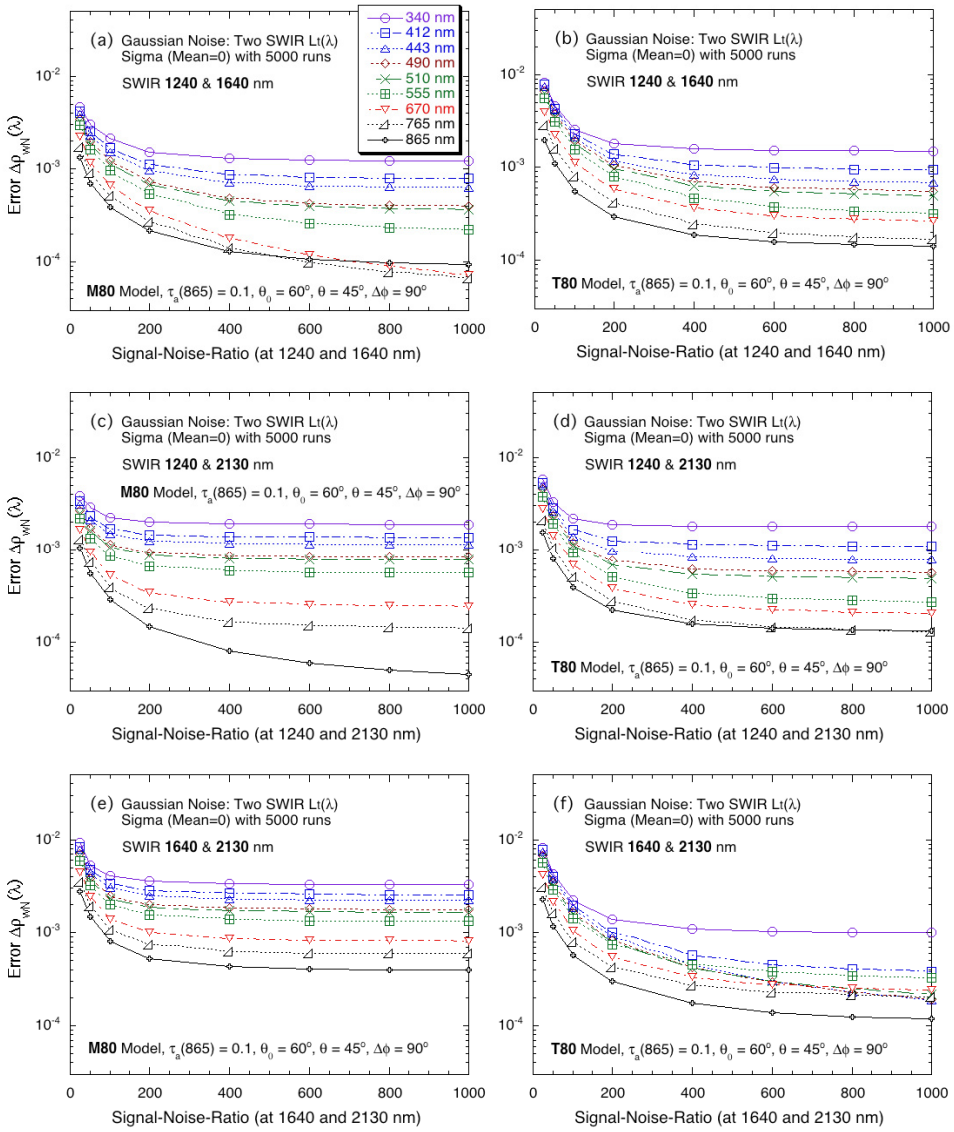

Fig. 4. Error $\Delta\rho_{wN}(\lambda)$ for wavelengths of the UV (340 nm) to red (670 nm) and NIR (865 nm) as a function of the SNR value using three SWIR atmospheric corrections for the M80 and T80 aerosol models with AOT at 865 nm of 0.1 for cases of (a) and (b) using the SWIR 1240 & 1640 nm for the M80 and T80 models, (c) and (d) using the SWIR 1240 & 2130 nm for the M80 and T80 models, and (e) and (f) using the SWIR 1640 and 2130 nm for the M80 and T80 models.

Again, similar to results in Figs. 2 and 3, results in Fig. 4 show that error $\Delta\rho_{wN}(\lambda)$ decreases with increase of the SNR value in the two corresponding SWIR bands that are used for atmospheric correction (or decrease of the sensor SWIR bands noise error). The error $\Delta\rho_{wN}(\lambda)$ reaches to the inherent SWIR atmospheric correction algorithm error [10] with large enough SNR values. For the SWIR atmospheric correction, it is quite apparent that when the

Optics EXPRESS

SNR reaches to ~200 for the three SWIR bands the error $\Delta\rho_{wN}(\lambda)$ gets close to the corresponding SWIR algorithm inherent errors (Fig. 4). This is particularly true for the UV (340 nm) and blue bands. With further increase of the SNR value (e.g., SNR of ~300–400), there are generally still some improvements in $\rho_{wN}(\lambda)$ for the red and NIR bands. However, with an SNR of ~200 for the SWIR bands, error $\Delta\rho_{wN}(\lambda)$ is already quite small for these bands (~10^{-4}) and improvements in $\rho_{wN}(\lambda)$ with further increase of SNR value from ~200 to ~300–400 is not significant. Considering the required resource to increase the SNR value for the SWIR bands, we set the sensor goal SWIR SNR requirement > ~200 for the SWIR atmospheric correction [10].

For the minimum requirement of the SWIR SNR values, results in Fig. 4 show that, when the SWIR SNR value is > ~100, almost all $\Delta\rho_{wN}(443)$ errors are ~1–2 × 10^{-3}, in particular, $\Delta\rho_{wN}(\lambda)$ values at the green, red, and NIR bands are significantly reduced to ~10^{-4}–10^{-3}. This is quite important because over turbid coastal and inland waters $\rho_{wN}(\lambda)$ spectra from the green to the NIR wavelengths are important parameters needed to well characterize the water optical, biological, and biogeochemical properties [30, 41, 42]. Thus, the minimum sensor SNR requirement for the three SWIR bands is > ~100, more or less consistent with results from *Wang* (2007) [10].

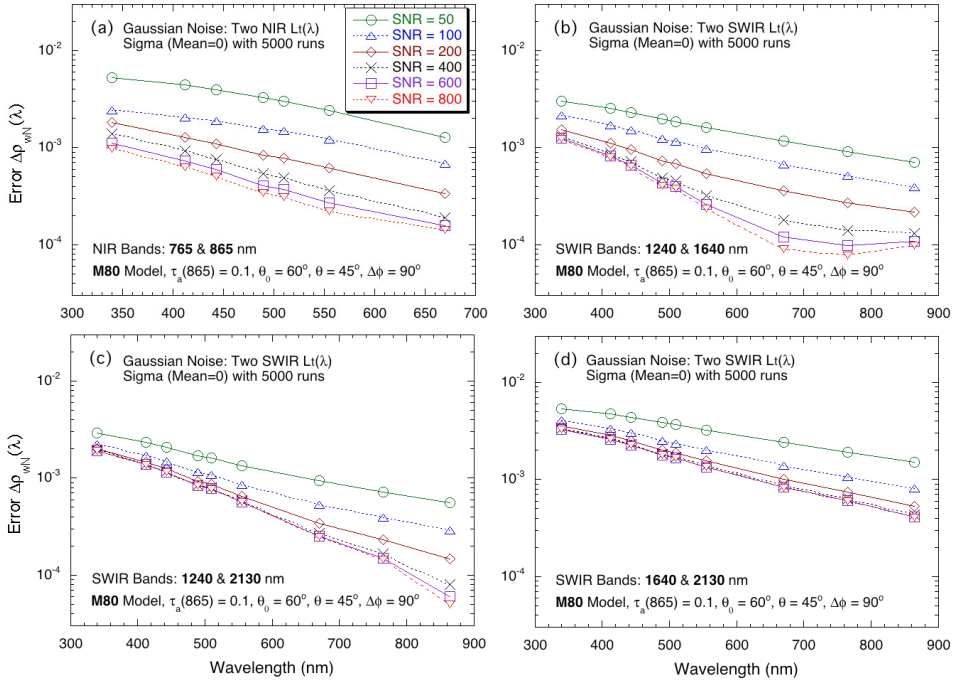

Fig. 5. Error $\Delta\rho_{wN}(\lambda)$ for the SNR value from 50 to 800 at the NIR and SWIR bands as a function of the wavelength for the M80 aerosol model with AOT at 865 nm of 0.1 for cases of atmospheric correction using (a) the two NIR bands at 765 and 865 nm, (b) the two SWIR bands at 1240 and 1640 nm, (c) the two SWIR bands at 1240 and 2130 nm, and (d) the two SWIR bands at 1640 and 2130 nm.

3.3. Comparison of SNR results for the NIR and SWIR atmospheric corrections

Figures 5 and 6 show results for $\Delta\rho_{wN}(\lambda)$ as a function of wavelength for aerosol models of the M80 (Fig. 5) and T80 (Fig. 6) for the NIR and the three SWIR atmospheric corrections with the SNR value from 50 to 800 for the corresponding NIR and SWIR bands that are used for atmospheric correction. It is noted that the wavelength scale (x-axis) is different for the NIR

Optics EXPRESS

and SWIR results as the SWIR results also include the NIR $\Delta\rho_{wN}(\lambda)$ data. First, it is quite obvious from Figs. 5 and 6 that the error $\Delta\rho_{wN}(\lambda)$ are strongly spectrally coherent, i.e., almost as a linear function of the wavelength in a logarithmic scale [11], increasing with decrease of the wavelength. Second, results from the NIR atmospheric correction [Figs. 5(a) and 6(a)] show clearly large error $\Delta\rho_{wN}(\lambda)$ with low SNR values (e.g., large differences among SNR curves of 50 to ~600), compared with results from the SWIR atmospheric corrections. It indeed shows that with the SNR of ~200–300 for the two NIR bands (the minimum NIR SNR requirement) error $\Delta\rho_{wN}(\lambda)$ are all within ~1–2 × 10^{-3} from the UV (340 nm) to the red (670 nm) [Figs. 5(a) and 6(a)]. On the other hand, for the SWIR bands with an SNR of ~100 (the minimum SNR requirement for the SWIR bands), the SWIR atmospheric corrections can produce error $\Delta\rho_{wN}(\lambda)$ ~1–2 × 10^{-3} [Figs. 5(b)–5(d) and Figs. 6(b)–6(d)]. Third, results in Figs. 5 and 6 show that effects of the SNR value at the NIR and SWIR bands depend also on the aerosol model (or aerosol type) as well as the SWIR band set used for atmospheric correction [10].

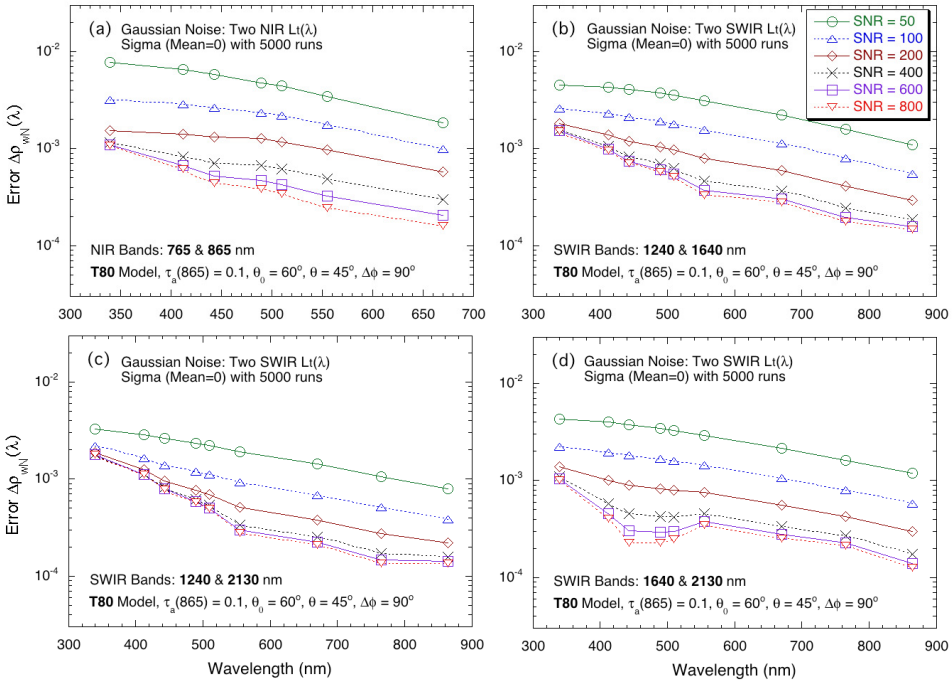

Fig. 6. Error $\Delta\rho_{wN}(\lambda)$ for the SNR value from 50 to 800 at the NIR and SWIR bands as a function of the wavelength for the T80 aerosol model with AOT at 865 nm of 0.1 for cases of atmospheric correction using (a) the two NIR bands at 765 and 865 nm, (b) the two SWIR bands at 1240 and 1640 nm, (c) the two SWIR bands at 1240 and 2130 nm, and (d) the two SWIR bands at 1640 and 2130 nm.

For the SWIR atmospheric correction using the SWIR band set of 1240 & 1640 nm, there are still some room to improve satellite-derived $\rho_{wN}(\lambda)$ spectra with the SWIR SNR increased from ~200 (the goal SNR requirement) to ~400 for both M80 and T80 aerosols [Figs. 5(b) and 5(b)]. Therefore, the goal SNR values between ~200–400 for the SWIR bands 1240 and 1640 nm are useful for further reducing data noise in satellite-derived $\rho_{wN}(\lambda)$ spectra. However, for cases of the SWIR band sets of 1240 & 2130 nm and 1640 & 2130 nm for atmospheric correction, an SNR value of ~200 at these SWIR bands is large enough for atmospheric correction, in particular, there are no gains to be achieved with further increase of SWIR SNR values [Figs. 5(c), 5(d), 6(c), and 6(d)]. In fact, results in Figs. 5(c) and 5(d)

Optics EXPRESS

show that, for atmospheric correction utilizing the SWIR band 2130 nm, a minimum of SNR value ~100 is required.

Finally, in the case of coastal waters, the results presented in Figs. 5 and 6 can be used to determine the required SNR values after being given acceptable values for $\Delta\rho_{wN}(\lambda)$ for the particular coastal area or process under study. In addition, investigators can use these results directly to determine the applicability of data from an existing sensor to their particular coastal study.

In summary, it is clear that a goal SNR ~200 should be assigned to the three SWIR bands.

4. Discussion

From extensive simulations, the sensor SNR requirements for the NIR and SWIR bands used for atmospheric correction for satellite ocean color remote sensing are derived. We provide two SNR values for the requirements for the NIR and SWIR bands: the minimum and the goal. The minimum SNR requirements are those for which an ocean color satellite sensor can produce sufficiently accurate ocean color products for general research and various applications. On the other hand, the goal SNR requirements are those for fully utilizing the standard atmospheric correction performance [9, 10, 40] for producing further improved ocean color data, in particular, significantly reducing ocean color product data noise. In fact, *Hu et al.* (2012) [43] have shown that MODIS-Aqua can produce much higher ocean color data quality than those from SeaWiFS because MODIS has much high SNR values in the two NIR bands (748 and 869 nm) compared with those of SeaWiFS (765 and 865 nm). In their estimations [43], MODIS-Aqua has SNR values for the two corresponding NIR bands at 748 and 869 nm of 995 and 806, respectively, while SNR values for the SeaWiFS two NIR bands at 765 and 865 nm are 219 and 183, respectively. Thus, MODIS-Aqua has the NIR SNR values actually exceeding the required goal SNR value of ~600, and SeaWiFS meets the required minimum NIR SNR value of ~200. Indeed, with the NIR SNR value ~200, SeaWiFS has provided reasonably good quality global ocean color data for scientific research and various applications [44]. However, some significant noise in the SeaWiFS-derived ocean color products is indeed quite obvious compared with those from MODIS-Aqua [43]. In fact, a recent study shows that the minimum SNR requirements for the visible can be reduced to ~400 when the NIR SNR values having ~600 [45]. VIIRS-SNPP has the estimated SNR values at the two NIR bands 745 and 862 nm about 368 and 457 [46], respectively. Therefore, VIIRS-SNPP should be able to provide sufficiently accurate ocean color products [8]. Actually, VIIRS-SNPP should be able to derive much better ocean color product data quality (reduced data noise) than those from SeaWiFS, although data noise may be slightly higher compared with those from MODIS-Aqua.

Because both MODIS and VIIRS SWIR bands are designed for the land and atmosphere applications (with large TOA radiances), SNR values for the corresponding three SWIR bands are quite low over oceans [46] and do not meet the minimum SWIR SNR requirements as discussed in the previous sections [47]. However, over highly turbid coastal and inland waters, it has been shown that MODIS-Aqua SWIR bands are still quite useful for the SWIR-based atmospheric correction for deriving water optical, biological, and biogeochemical properties [48, 49], as well as for various studies and applications [50, 51].

We must emphasize that the results presented here depend on the atmospheric correction algorithm that has been used to process data from all U.S. ocean color satellite instruments [9, 10]. Algorithms used with other sensors, e.g., MERIS and OLCI [12], are variants that differ only in specific implementation details but not in the basic concept: use spectral bands for which $\Delta\rho_{wN}(\lambda)$ is negligible (NIR or SWIR) to assess the properties of the aerosol and then extrapolate the aerosol contribution to the visible using aerosol models and radiative transfer computations. Clearly, a new and improved algorithm will require a re-evaluation of the question of SNR requirements.

Optics EXPRESS

5. Summary

Assuming a Gaussian distribution for the sensor noise, some extensive simulations have been carried out to understand the effects of sensor noise error in the NIR and SWIR bands on atmospheric correction performance in deriving ocean $\rho_{wN}(\lambda)$ spectra. The simulations assume that the standard atmospheric correction algorithms [9, 10] are used for deriving satellite ocean color products, i.e., atmospheric correction uses either two NIR bands [9] or two SWIR bands [10] for the global ocean color data processing. The minimum and goal SNR requirements for the NIR and SWIR bands are assessed and derived. Results show that for the two NIR bands (e.g., at around 765 and 865 nm) the minimum SNR requirement is ~200–300, while the goal for the two NIR bands is ~600. For the SWIR atmospheric correction, with the caveat that coastal areas have highly varied optical characteristics, the minimum sensor SNR requirement for the three SWIR bands (e.g., at around 1240, 1640, and 2130 nm) is ~100, while the goal is ~200.

Acknowledgments

The views, opinions, and findings contained in this paper are those of the authors and should not be construed as an official NOAA or U.S. Government position, policy, or decision.